PASJ: Publ. Astron. Soc. Japan , 1–??,
© 2016. Astronomical Society of Japan.

arXiv:1602.05258v1 [astro-ph.SR] 17 Feb 2016

Oxygen abundance determination of B-type stars with the O I 7771–5 Å lines *

Yoichi TAKEDA[1,2] and Satoshi HONDA[3]
[1]*National Astronomical Observatory, 2-21-1 Osawa, Mitaka, Tokyo 181-8588*
takeda.yoichi@nao.ac.jp
[2]*SOKENDAI, The Graduate University for Advanced Studies, 2-21-1 Osawa, Mitaka, Tokyo 181-8588*
[3]*Nishi-Harima Astronomical Observatory, Center for Astronomy, University of Hyogo, 407-2 Nishigaichi, Sayo-cho, Sayo, Hyogo 679-5313*

(Received 2016 January 7; accepted 2016 February 15)

Abstract

Oxygen abundances of 34 B-type stars in the effective temperature range of $T_{\rm eff} \sim$ 10000–28000 K with diversified rotational velocities ($v_{\rm e} \sin i \sim$ 0–250 km s^{-1}) were determined from the O I triplet lines at 7771–5 Å, with an aim to examine whether this O I feature can be a reliable abundance indicator for such high-temperature stars including rapid rotators. It revealed that the required non-LTE abundance correction is distinctly large (ranging from ~ -0.6 dex to ~ -1.7 dex) and its consideration is indispensable. On the condition that the non-LTE effect is taken into account, this triplet is a useful O abundance indicator (with a precision of $\lesssim 0.2$ dex) up to $T_{\rm eff} \lesssim 25000$ K, since its total equivalent width is sufficiently large ($\gtrsim 200$ mÅ). In contrast, it is not adequate for abundance derivation for stars at $T_{\rm eff} \gtrsim 25000$ K, where its strength rapidly drops down toward a hardly detectable level (except for sharp-lined stars) and its sensitivity to $T_{\rm eff}$ or $\log g$ becomes considerably large. The resulting non-LTE oxygen abundances turned out to be almost normal (i.e., near-solar around $\sim$ 8.7–8.8 within $\sim \pm$ 0.2 dex) for most stars without any dependence upon projected rotational velocity as well as luminosity (or mass), which is consistent with the prediction of recent stellar evolution calculations.

Key words: line: formation — stars: abundances — stars: atmospheres — stars: early-type — stars: rotation

1. Introduction

The O I triplet lines at 7771–5 Å (3s ^{5}S$^{\rm o}$–3p ^{5}P, multiplet 1) are known to play important roles in stellar spectroscopy, since they are sufficiently strong to be visible in stars of wide temperature range (spectral types from K to B) and provide us with possibilities of studying not only oxygen abundances but also line-broadening parameters (such as turbulences or projected rotational velocities). Making use of this merit, our group has been exploited these lines for investigating the behavior of microturbulent velocities in A–F stars (Takeda 1992) as well as the O abundances of A–F dwarfs (Takeda & Sadakane 1997; Takeda et al. 2008), G–K giants (Takeda, Kawanomoto, & Sadakane 1998; Takeda et al. 2015), and M 67 stars from the turn-off point through the red-giant branch (Takeda & Honda 2015). This time we pay our attention to B-type stars, while expecting a usefulness of applying this O I triplet also to this high-temperature regime.

Studying surface oxygen abundances in B-type stars (which have comparatively high $T_{\rm eff}$ and M) is especially significant in connection with rapid rotators, since a deep mixing caused by the meridional circulation may salvage ON-cycled material from the interior to produce more or less an underabundance of O at the surface, similarly to an overabundance of He due to mixing of H→He processed product. Since rapidly-rotating B-type stars showing He-enhancement are actually observed (e.g., Lyubimkov et al. 2004), O-deficiency may be another indicator for the existence of efficient rotation-induced mixing, and thus observational information on the oxygen abundances of a large number of B-type stars with various rotational velocities can make an important touchstone for the prediction from the stellar evolution theory (e.g., Georgy et al. 2013).

On the observational side, oxygen abundances of B-type stars have so far been studied mainly by using O II lines in the blue region (see, e.g., Gies & Lambert 1992; Kilian 1992; Cunha & Lambert 1994; Korotin, Andrievsky, & Luck 1999; Simón-Díaz 2010; Nieva & Przybilla 2012; Lyubimkov et al. 2013), Although these ionized oxygen lines are useful because they are numerous in number, their application is exclusively limited to early B stars, since the strengths of these lines quickly fall off below $T_{\rm eff} \sim$ 20000 K. This is a shortcoming from a viewpoint of continuation/comparison with lower temperature stars (A, F, and G types), for which neutral O I lines have to be used. Besides, since these previous studies using O II lines are mostly directed to sharp-lined B stars, prospect for applying them to rapid rotators is not clear.

Meanwhile, spectroscopic investigations on the O abundances of B-type stars using neutral oxygen lines have

* Based on data collected by using the NAYUTA Telescope of the Nishi-Harima Astronomical Observatory.

been less common and tend to be biased to either late-B stars or slow rotators. Takeda et al. (2010; hereinafter referred to as Paper I) carried out a non-LTE analysis on the O (and Ne) abundances of sharp-lined B stars ($v_{\rm e}\sin i \sim$ 0–30 km s^{-1} and 10000 K $\lesssim T_{\rm eff} \lesssim$ 23000 K) by using O I 6156–8 lines (multiplet 10), which however are inapplicable to rapid rotators because of their weakness. Niemczura, Morel, and Aerts's (2009) LTE study on the abundances of oxygen (along with other elements) based on weaker O I lines[1] is limited to B6–B9.5 stars. Similarly, only late-B (B5–B9) stars were targeted in Hempel and Holweger's (2003) determination of non-LTE oxygen abundances based on O I 7771-5 lines.

Among the previous abundance studies of B-type stars, most notable in connection with our present interest would be the recent one of Nieva and Przybilla (2012), who determined the abundance of O (along with those of He, C, N, Ne, Mg, Si, and Fe) for 20 sharp-lined mid-to-early B stars (16000 K $\lesssim T_{\rm eff} \lesssim$ 33000 K) by using the state-of-the-art non-LTE technique based on high-S/N and high-resolution spectra. While their analysis mainly depends on a number of O II lines, they also employed O I lines (e,g., O I features at 6156–8 Å, 7771–5 Å, and 8446 Å) for stars with $T_{\rm eff} \lesssim$ 27000 K, in order to check that O I/O II ionization equilibrium is accomplished. Although their work is regarded as an important benchmark, only apparently slow rotators ($v_{\rm e}\sin i \lesssim$ 30 km s^{-1}) were treated and rapid rotators were out of their consideration.

This situation motivated us to investigate a possibility of applying O I 7771–5 lines to B stars with much wider range stellar properties; i.e., $T_{\rm eff} \sim$ 10000–30000 K corresponding to late B through early B type, slow as well as rapid rotators covering $0 \lesssim v_{\rm e}\sin i \lesssim$ 200–300 km $^{-1}$.
— Is this O I triplet feature still usable for early B-type stars ($T_{\rm eff} \sim$ 20000–30000 K) of various rotational velocities, despite that its strength should be considerably weakened as most O atoms are ionized at such high $T_{\rm eff}$ range?
— How is the behavior of its strength in terms of the stellar parameters; e.g., $T_{\rm eff}$, surface gravity ($\log g$), microturbulence (ξ), and oxygen abundance? Is it suitable for abundance determination?
— How much important is the non-LTE effect regarding this strong O I triplet? Does the required non-LTE abundance correction depend on the atmospheric parameters?

Toward answering these questions, we first conducted non-LTE calculations on an extensive parameter grid in order to understand how the O I 7771–5 strengths of B stars behave in terms of various key parameters, and then carried out an observational study of non-LTE oxygen abundance determinations for 34 selected late-B through early-B type stars with diversified $v_{\rm e}\sin i$ values based on the spectra newly obtained at Nishi-Harima Astronomical Observatory. The purpose of this paper is to report the consequence of this investigation.

The remainder of this article is organized as follows: The observational data of our program stars are described in section 2, and their spectroscopic parameters are derived in section 3. We explain our non-LTE calculations in section 4, and the procedures of abundance determination (including profile fitting, equivalent width evaluation, and error estimation) in section 5. The resulting behavior of non-LTE correction and the trend of oxygen abundances of B-type stars are discussed in section 6, followed by section 7 where the conclusions are summarized.

2. Observational data

The list of our 34 targets is presented in table 1, all of which are apparently bright ($V \leq 5$ mag) and selected from the extensive $v_{\rm e}\sin i$ compilation of 1092 northern B-type stars published by Abt, Levato, and Grosso (2002), where B supergiants and Be stars were excluded from our selection. Our sample includes stars of diversified $v_{\rm e}\sin i$ values (from slow rotators to rapid rotators up to $v_{\rm e}\sin i \sim$ 200 km s^{-1}). These program stars are plotted on the $\log L$ vs. $\log T_{\rm eff}$ diagram (theoretical HR diagram) in figure 1, where Girardi et al.'s (2000) theoretical evolutionary tracks corresponding to different stellar masses are also depicted. We can see from this figure that the masses of our sample stars are in the range between $\sim 2.5 M_\odot$ and $\sim 15 M_\odot$.

Spectroscopic observations of these stars were carried out in the summer season of 2015 (May through September; observation date for each star is given in table 1) by using the Medium And Low-dispersion Longslit Spectrograph (MALLS; cf. Ozaki & Tokimasa 2005) installed on the Nasmyth platform of the 2 m NAYUTA telescope at Nishi-Harima Astronomical Observatory (NHAO). Equipped with a 2K×2 K CCD detector (13.5 μm pixel), MALLS can record a spectrum covering $\sim$ 400 Å (7600–8000 Å) in the medium-resolution mode with the resolving power of $R \sim$ 12000. While the exposure time of one frame was typically a few minutes, several spectral frames were co-added to improve the signal-to-noise ratio. The reduction of the spectra (bias subtraction, flat-fielding, spectrum extraction, wavelength calibration, co-adding of frames to improve S/N, continuum normalization) was performed by using the "noao.onedspec" package of the software IRAF[2] in a standard manner. The S/N ratios of the resulting spectra were estimated to be around $\sim$ 200–300 in most cases (except for HR 0779, for which S/N is only $\sim$ 60–70), which turned out to be sufficient for our purposes. Our final spectra in the 7700–7850 Å region for each of the 34 stars are shown in figure 2.

3. Atmospheric parameters

The effective temperature and the surface gravity of each program star were determined from the colors of Strömgren's $uvby\beta$ photometric system with the

[1] Although they did not explicitly publish the list of used lines, they must have exploited weaker O I lines (presumably those at 6156–8 Å), since they stated that O I 7771–5 lines were excluded because of the strong non-LTE effect.

[2] IRAF is distributed by the National Optical Astronomy Observatories, which is operated by the Association of Universities for Research in Astronomy, Inc. under cooperative agreement with the National Science Foundation.

help of Napiwotzki, Scönberner, and Wenske's (1993) `uvbybetanew` program,[3] where the observational data of $b-y$, c_1, m_1, and β were taken from Hauck and Mermilliod (1998) via the SIMBAD database. The resulting $T_{\rm eff}$ and $\log g$ are summarized in table 1. The model atmosphere for each star was then constructed by two-dimensionally interpolating Kurucz's (1993) ATLAS9 model grid in terms of $T_{\rm eff}$ and $\log g$, where we exclusively applied the solar-metallicity models.

As to typical errors of these parameters, we may estimate $\sim 3\%$ in $T_{\rm eff}$ and ~ 0.2 dex in $\log g$ for most of our sample stars (i.e., 32 stars at 10000 K $\lesssim T_{\rm eff} \lesssim$ 24000 K) according to Napiwotzki et al. (1993; cf. section 5 therein). We should note, however, that parameters derived from Napiwotzki et al.'s code would not be reliable any more for stars at $T_{\rm eff} > 24000$ K, as pointed out by Nieva (2013) based on the results of Nieva and Przybilla (2012) who used non-LTE ionization equilibria of various species along with the profiles of Balmer lines to determine the atmospheric parameters. Accordingly, the parameters of the relevant two stars (HR 8238 and HR 8797; cf. table 1) having particularily high $T_{\rm eff}$ (25231 K and 27853 K, respectively) should be viewed with caution and their errors may be larger than the typical amounts mentioned above.

Given that HR 779 (HD 16582) and HR 8238 (HD 205021) in our sample were also studied by Nieva and Przybilla (2012), it is interesting to compare our color-based $T_{\rm eff}$ and $\log g$ with their spectroscopically determined values which may be more reliable. The results of ($T_{\rm eff}^{\rm ours}/T_{\rm eff}^{\rm Nieva}$, $\log g^{\rm ours}/\log g^{\rm Nieva}$) are (21747/21250, 3.63/3.80) for HR 779 and (25231/27000, 3,63/3.95) for HR 8238. We can see a reasonable consistency within the expected errors for the former B2 star ($T_{\rm eff} < 24000$ K), while the discrepancy is larger for the latter B0.5 star ($T_{\rm eff} > 24000$ K) which may be attributed to the reason mentioned above (i.e., outside of the reliability limit of Napiwotzki et al.'s calibration).

Regarding the microturbulence, which is necessary for abundance determination, we had to assign an appropriate value since it was not possible to establish this parameter based on our spectra. Here, we divide our targets into two classes of $T_{\rm eff} < 15000$ K and $T_{\rm eff} > 15000$ K, and tentatively assume $\xi = 1(\pm 1)$ km s^{-1} for the former and $\xi = 3(\pm 2)$ km s^{-1} for the latter, based on the discussion in Takeda et al. (2014; cf. section 3 therein) and Paper I (cf. section 3 therein), respectively. Admittedly, this is a rather rough choice; but it appears to be reasonable as will be discussed in subsection 6.2.

4. Non-LTE calculations

In order to evaluate the non-LTE effect on the strength of O I 7771–5 triplet, we carried out non-LTE calculations for oxygen on an extensive grid of solar-metallicity model atmospheres resulting from combinations of eleven $T_{\rm eff}$ values (9000, 10000, 12000, 14000, 16000, 18000, 20000, 22000, 24000, 26000, 28000 K) and four $\log g$ values (3.0, 3.5, 4.0, 4.5),[4] which sufficiently cover the parameter ranges of our program stars. The statistical equilibrium calculations for oxygen were done in the same manner as in Paper I (cf. subsection 4.1 therein). Our non-LTE calculation program is based on the code described in Takeda (1991). The atomic model of oxygen is the same as that adopted by Takeda (2003; cf. subsection 2.1 therein), which is based on the atomic data given in Kurucz and Bell (1995). Other various fixed collisional and radiative rates were evaluated as described in Takeda (1992). The non-LTE departure coefficients [$b(\tau)$] applied to each star (to be used for non-LTE abundance determination in section 5) were then derived by two-dimensionally interpolating this grid in terms of $T_{\rm eff}$ and $\log g$, as was done for model atmospheres.

Toward understanding the behavior of the non-LTE effect to be discussed in subsection 6.1, theoretical non-LTE and LTE equivalent widths ($W_{\rm N}$ and $W_{\rm L}$) of the whole triplet were computed on this grid of models for combinations of four oxygen abundances ([O/H][5] $= -0.6$, -0.3, 0.0, and $+0.3$) and three microturbulences ($\xi = 1$, 3, and 5 km s^{-1}) by using Kurucz's (1993) WIDTH9 program[6] with the atomic data presented in table 2, where W was evaluated by directly integrating the synthesized profiles of triplet lines over the wavelength region between 7770.44 Å and 7776.94 Å (i.e., 1.5 Å margin both shortward of the 7771.94 line and longward of the 7775.39 line). We also evaluated the corresponding non-LTE abundance corrections (Δ) defined as $A_{\rm N} - A_{\rm L}$, where $A_{\rm N}$ and $A_{\rm L}$ are the abundances derived by inversely analyzing $W_{\rm N}$ in non-LTE and LTE, respectively. The resulting W and Δ values are summarized in the electronic data tables (file name: ncor7773_xi?.dat) available as on-line materials. The behaviors of the computed W and δ in terms

[3] ⟨http://www.astro.le.ac.uk/~rn38/uvbybeta.html⟩.

[4] Since ATLAS9 model grid does not include $\log g = 3.0$ models at $T_{\rm eff} \geq 27000$ K presumably because of an instability problem, models of only three gravities ($\log g = 3.5$, 4.0, and 4.5) could be used for $T_{\rm eff} = 28000$ K.

[5] [O/H] [$\equiv A_{\rm star}$(O) $-A_{\odot}$(O)] is the differential logarithmic oxygen abundance relative to the Sun, where A is defined in the usual normalization of A(H) = 12.00 and we employed $A_{\odot}$(O) = 8.93 in order to maintain consistency with the similar non-LTE grid computed by Takeda (2003) for FGK stars. Note that this reference solar abundance (8.93), which was taken from Anders and Grevesse (1989) and adopted as the standard value in the ATLAS9 program, is appreciably higher by Asplund et al.'s (2009) recently updated value (8.69) based on their 3D hydrodynamical solar model photosphere. However, it is closer to the solar non-LTE oxygen abundance (8.81) derived by Takeda and Honda (2005) with the same O I 7771–5 lines (see the discussion in subsection 5.1 of Paper I).

[6] The original WIDTH9 program had been considerably modified in various respects. In order to enable simulation of line profiles by taking into account the non-LTE effect, the LTE line opacity and the LTE line source function usually used in the WIDTH9 program were multiplied by the depth-dependent NLTE-to-LTE line opacity ratio ($l_0^{\rm NLTE}/l_0^{\rm LTE}$) and the NLTE line source function ratio ($S_{\rm L}/B$) resulting from our non-LTE calculation code, respectively (cf. subsection 4.2 in Takeda 1991 for more details). Besides, since the original WIDTH9 program can handle only a single isolated line, a spectrum synthesis technique was incorporated for calculating the total equivalent width of a multi-component feature (such as O I 7771–5).

of the atmospheric parameters are shown in figure 3 for selected representative cases, on which we will focus later in subsection 6.1.

5. Abundance determination

As in Paper I, our strategy of determining the abundance and related quantities (e.g., non-LTE correction, uncertainties due to ambiguities of atmospheric parameters) consists of the following consecutive steps: (i) derivation of provisional abundance solution by applying the spectrum-fitting technique, (ii) evaluation of the equivalent width (W) by using this fitting-based abundance, and (iii) analysis of such derived W with the standard parameters and changing the conditions (perturbed parameters, LTE and non-LTE).

5.1. Synthetic spectrum fitting

We first searched for the solutions for the oxygen abundance (A), projected rotational velocity ($v_{\rm e}\sin i$), and radial velocity ($V_{\rm rad}$) such as those accomplishing the best fit (minimizing $O-C$ residuals) between the theoretical and observed spectrum in the $\sim$ 7765–7780 Å region, while applying the automatic fitting algorithm (Takeda 1995). In this preparatory step, we used the model atmosphere (cf. section 3) and the non-LTE departure coefficients (section 4) prepared for each star but adopted the same microturbulence of $\xi = 3$ km s^{-1} for computing the non-LTE theoretical spectrum. Regarding the macroscopic line-broadening function to be convolved with the intrinsic spectrum, we included the instrumental broadening (assumed to be the Gaussian function) corresponding to $R \sim 12000$ and the rotational broadening with the limb-darkening coefficient of $\epsilon = 0.3$ (estimated from Fig. 17.6 of Gray 2005) How the theoretical spectrum for the converged solutions fits well with the observed spectrum is demonstrated in figure 4.[7] The resulting $v_{\rm e}\sin i$ values are presented in table 1, which are also compared with those given in Abt et al.'s (2002) catalogue in figure 5.

5.2. Derivation and analysis of equivalent width

Next, we inversely computed the equivalent width (W) for the whole O I 7771–5 triplet (as done in section 4) by using the abundance solution (derived from the fitting analysis) along with the same model atmosphere/parameters. Based on such evaluated W value, the non-LTE abundance ($A_{\rm N}$) as well as LTE abundance ($A_{\rm L}$) were freshly computed by applying the microturbulence assigned to each star (1 or 3 km s^{-1} depending on $T_{\rm eff}$; cf. section 3), from which the non-LTE correction (Δ) was further derived. These W, $A_{\rm N}$, and Δ values are also given in table 1.

[7] Note that, in the evaluation of $O-C$ residuals, we sometimes masked some regions showing features irrelevant to stellar spectra, such as spurious spectrum defect, as highlighted in green in this figure.

5.3. Sensitivity to parameter perturbation

We also estimated the errors in $A_{\rm N}$ caused by ambiguities involved in the standard atmospheric parameters (presented in table 1). Since their typical uncertainties are $\pm$3% in $T_{\rm eff}$, $\pm$0.2 dex in $\log g$, and $\pm$1 km s^{-1} (for $T_{\rm eff} < 15000$ K) or $\pm$2 km s^{-1} (for $T_{\rm eff} > 15000$ K) in ξ (cf. section 3). six kinds of abundance variations (δ_{T+}, δ_{T-}, δ_{g+}, δ_{g-}, $\delta_{\xi+}$, and $\delta_{\xi-}$) were derived by repeating the analysis on the W values while perturbing the standard atmospheric parameters interchangeably by these amounts. Finally, the root-sum-square of these perturbations, $\delta_{Tg\xi} \equiv (\delta_T^2 + \delta_g^2 + \delta_\xi^2)^{1/2}$, was regarded as the abundance uncertainty (due to combined errors in $T_{\rm eff}$, $\log g$, and ξ), where δ_T, δ_g, and δ_ξ are defined as $\delta_T \equiv (|\delta_{T+}| + |\delta_{T-}|)/2$, $\delta_g \equiv (|\delta_{g+}| + |\delta_{g-}|)/2$, and $\delta_\xi \equiv (|\delta_{\xi+}| + |\delta_{\xi-}|)/2$, respectively. The resulting abundances ($A_{\rm N}$), equivalent widths (W), non-LTE corrections (Δ), and abundance variations (δ's) in response to parameter changes, are graphically displayed as functions of $T_{\rm eff}$ in figure 6, which we will discuss in subsection 6.2.

6. Discussion

6.1. Behavior of line strength and non-LTE correction

Before discussing the results of our analysis derived in section 5 for the program stars, we first review how the strength of O I 7771–5 triplet and its non-LTE effect behaves in terms of the atmospheric parameters. The following characteristics can be summarized by inspection of figure 3:

— Generally, W declines with an increase in $T_{\rm eff}$. While its change is gradual at $T_{\rm eff} \lesssim 25000$ K, a rather abrupt drop of W occurs at $T_{\rm eff} \gtrsim 25000$ K where oxygen is predominantly ionized and very few neutral oxygen atoms remain.

— Naturally, W increases with an increase in [O/H] and ξ, though it is almost ξ-independent at $T_{\rm eff} \gtrsim 25000$ K where the line is weak in the linear part of the curve of growth.

— The behavior of W in response to changing $\log g$ is somewhat complicated (figure 3c). While the line strength slightly grows with a lowering of $\log g$ at $T_{\rm eff} \lesssim 25000$ K (because of the increased non-LTE effect; note that this tendency is seen only in $W_{\rm N}$ but not in $W_{\rm L}$), the trend is reversed at $T_{\rm eff} \gtrsim 25000$ K where W markedly weakens with a decrease in $\log g$ because the effect of enhanced ionization becomes more important at the condition of lower-density.

— The non-LTE effect always acts in the direction of intensifying the line strength ($W_{\rm N} > W_{\rm L}$), which makes the non-LTE abundance correction (Δ) always negative.

— The extent of $|\Delta|$ has a peak at $T_{\rm eff} \sim$ 15000–20000 K and tends to be larger for higher [O/H], smaller ξ, and lower $\log g$, which can be interpreted that the non-LTE effect becomes more significant when the line-forming depth is higher or in the lower density region.

6.2. Trend of oxygen abundances

We now discuss figure 6. The equivalent widths (W) derived in subsection 5.2 show a decreasing trend with an increase in $T_{\rm eff}$ (figure 6a), which is reasonably consistent with the theoretically predicted trend for $W_{\rm N}$ (cf. figure 3a–c).

The $|\Delta|$ values are in the range of $\sim$ 0.6–1.7 dex (figure 6b), which are so large that these corrections are indispensable for reliable determination of oxygen abundances of B-type stars based on the O I 7771–5 lines. Comparing these results with those of Hempel and Holweger (2003), who determined the non-LTE oxygen abundances of B5–B9 stars ($T_{\rm eff} \sim$ 9000–17000 K) based on the same O I triplet, we see that their $|\Delta|$ values ($\sim$ 0.3–1.2; cf. their table 5) are considerably smaller than ours. We suspect that they underestimated the importance of the non-LTE effect, which may explain the significantly supersolar $[{\rm O/H}]_{\rm NLTE}$ results (by $\sim$ +0.3–0.6 dex) they obtained for many of their sample stars.

Figure 6c suggests that the oxygen abundances derived for the 34 B-type stars distribute around $\sim$ 8.7–8.8 without any systematic $T_{\rm eff}$-dependence. Actually the average abundance over all 34 stars makes $\langle A \rangle = 8.72$ (with standard deviation $\sigma = 0.16$). If three stars with $A({\rm O}) < 8.4$ (HR 6779, 7236, 8238) showing appreciable deviations are excluded, we have $\langle A \rangle = 8.76$ ($\sigma = 0.10$). This means that the surface oxygen abundances of these B-type stars are mostly near to the solar composition (see footnote 5), which is in fairly good agreement with the previous studies for B-type stars; e.g., 8.71 ± 0.06 derived in Paper I based on O I 6156–8 lines or 8.73 ± 0.13 by Lyubimkov et al. (2013) based on O II lines (see also table 6 and table 7 therein).

Regarding the abundance errors caused by uncertainties in atmospheric parameters, δ_ξ ($\sim$ 0.1–0.2 dex) is predominantly important over δ_T (< 0.1) or δ_g (< 0.1) at $T_{\rm eff} \lesssim$ 25000 K, to which most of the program stars are relevant (cf. figure 6d–f). Accordingly, the extents of $\delta_{tg\xi}$ (error bars attached to the symbols in figure 6c) are essentially determined by δ_ξ and on the order of $\sim$ 0.1-0.2 dex (except for the two stars of $T_{\rm eff} \gtrsim$ 25000 K), which is consistent with the standard deviation of our abundance results. It may appropriate here to comment on the assigned values of ξ mentioned in section 3. Since the abundances derived for given microturbulences of $\xi = 1(\pm1)$ km s^{-1} ($T_{\rm eff} < 15000$ K) and $\xi = 3(\pm2)$ km s^{-1} ($T_{\rm eff} > 15000$ K) do not show any systematic trend in terms of $T_{\rm eff}$, this may imply that our choice is reasonably justified. If a constant ξ were assigned for all stars, we would have obtained a spurious $T_{\rm eff}$-dependence.[8]

The oxygen abundances of 34 stars are plotted against $v_{\rm e} \sin i$ as well as $\log L$ in figure 7, where we can not see any systematic dependence. This means that no appreciable O abundance anomaly is detected in our sample stars at least within the precision of $\lesssim$ 0.1–0.2 dex. According to Georgy et al.'s (2013) calculation, while no change in the surface composition is produced at all during the main sequence period for the case of non-rotating stars, rapidly rotating stars may show some abundance peculiarities caused by the rotational mixing of nuclear processed product. For example, regarding the cases of solar-metallicity ($Z = 0.014$) models, the changes of He|O abundances at the end of the main sequence for 4 $M_\odot$ star is +0.2%|−0.7% ($\Omega/\Omega_{\rm crit} = 0.5$) and +3.1%|−6.2% ($\Omega/\Omega_{\rm crit} = 0.95$), while those for 9 $M_\odot$ star is +1.9%| − 4.9% ($\Omega/\Omega_{\rm crit} = 0.5$) and +11.4%| − 17.3% ($\Omega/\Omega_{\rm crit} = 0.95$), where $\Omega_{\rm crit}$ is the angular rotational velocity corresponding to the critical break-up. However, even if such an abundance change as large as $\sim$ 20% exists, it corresponds to only $\lesssim$ 0.1 dex in the logarithmic scale. Thus, it is no wonder that we could not detect such a subtle amount, given that the precision of our abundance determination is $\lesssim$ 0.2 dex. In this sense, we may state that our result is more or less consistent with the recent stellar evolution calculations based on the canonical mixing theory.

6.3. Usability of O I triplet lines for abundance determination

Finally, we turn to the question which motivated this investigation (cf. section 1): Is the O I 7771–5 triplet practically useful for oxygen abundance determination of B-type stars? Our answer is as follows:

— Yes, it is surely useful as far as stars of $T_{\rm eff} \lesssim$ 25000 K are concerned (given that the non-LTE effect is properly taken into account), since its strength is still sufficiently large ($W \gtrsim 200$ mÅ) and abundances are not seriously affected by uncertainties in the atmospheric parameters.

— For example, if we consider a case of $v_{\rm e} \sin i \sim 300$ km s^{-1} and $W \sim 200$ mÅ, the FWHM and the central depth of the merged triplet feature would be ~ 10 Å and ~ 2%, respectively, which is measurable without difficulty on a spectrum with S/N ratios of a few hundred.

— In contrast, regarding very early B stars of $T_{\rm eff} \gtrsim$ 25000 K (corresponding to $\sim$ B0), the strength of this triplet quickly drops away and its sensitivity to ambiguities of $T_{\rm eff}$ or $\log g$ becomes seriously large, which makes it unsuitable as a reliable abundance indicator.

— We should keep in mind, however, even for the well-behaved case of $T_{\rm eff} \lesssim$ 25000 K stars, the precision of abundance derivation would be on the order of $\lesssim$ 0.2 dex, which is mainly restricted by uncertainties in the choice of microturbulence. Accordingly, very high-precision should not be expected.

— In this sense, detection of surface oxygen abundance anomaly based on these O I lines would be feasible only if the extent of peculiarity is sufficiently large (e.g., by $\sim$ 0.3 dex), such as the case where non-canonical deep mixing is relevant. The slight abundance change (up to $\lesssim$ 0.1 dex) predicted by the current canonical rotational mixing theory can hardly be detected.

[8] Actually, the first provisional abundances derived from the spectrum synthesis by tentatively using $\xi = 3$ km s^{-1} (cf. subsection 5.1) showed a tendency of appreciable underabundance in late B-type stars.

7. Summary and conclusion

In order to examine whether the O I triplet lines at 7771–5 Å can be used as a reliable oxygen abundance indicator for B-type stars of high $T_{\rm eff}$ including rapid rotators, we carried out oxygen abundance determinations for selected 34 B-type stars based on the spectra ($R \sim 12000$) obtained by the 2 m NAYUTA Telescope at Nishi-Harima Astronomical Observatory.

Regarding the atmospheric parameters, $T_{\rm eff}$ and $\log g$ were determined from $uvby\beta$ colors and the microturbulence was assumed to be $\xi = 1(\pm 1)$ km s^{-1} ($T_{\rm eff} < 15000$ K) and $\xi = 3(\pm 2)$ km s^{-1} ($T_{\rm eff} > 15000$ K) by consulting previous studies. The non-LTE effect was properly taken into consideration based on our non-LTE calculations carried out for an extensive grid of models.

We first determined the provisional abundance and $v_{\rm e} \sin i$ by applying the synthetic spectrum-fitting analysis to the 7771–5 feature, and then inversely determined (from the tentative abundance) the equivalent width of the whole triplet to be used for further evaluations of non-LTE/LTE abundances, non-LTE correction, and errors due to ambiguities of atmospheric parameters.

It was found that the extent of the (negative) non-LTE correction is appreciably large to be $|\Delta| \sim 0.6$–1.7 dex and its consideration is indispensable. The resulting non-LTE oxygen abundances turned out to be nearly solar ($\langle A \rangle \sim 8.7$–$8.8$ with $\sigma \lesssim 0.2$ dex) without any clear dependence upon rotation as well as luminosity (or mass), which is consistent with the results of published observational studies and stellar evolution calculations with the canonical mixing theory.

We concluded that this triplet is a useful O abundance indicator (with a precision of $\lesssim 0.2$ dex) up to $T_{\rm eff} \lesssim 25000$ K, since its total equivalent width is sufficiently large ($\gtrsim 200$ mÅ). In contrast, it is not adequate for abundance determination for stars at $T_{\rm eff} \gtrsim 25000$ K, where its strength rapidly turns down and its sensitivity to $T_{\rm eff}$ or $\log g$ becomes considerably large.

This research has made use of the SIMBAD database, operated by CDS, Strasbourg, France.

References

Abt, A. A., Levato, H., & Grosso, M. 2002, ApJ, 573, 359
Anders, E., & Grevesse, N. 1989, Geochim. Cosmochim. Acta, 53, 197
Arenou, F., Grenon, M., & Gómez, A. 1992, A&A, 258, 104
Asplund, M., Grevesse, N., Sauval, A. J., & Scott, P. 2009, ARA&A, 47, 481
Cunha, K., & Lambert, D. L. 1994, ApJ, 426, 170
ESA 1997, The Hipparcos and Tycho Catalogues, ESA SP-1200, available from NASA-ADC or CDS in a machine-readable form (file name: hip_main.dat)
Flower, P. J. 1996, ApJ, 469, 355
Girardi, L., Bressan, A., Bertelli, G., & Chiosi, C. 2000, A&AS, 141, 371
Georgy, C., Ekström, S., Granada, A., Meynet, G., Mowlavi, N., Eggenberger, P., & Maeder, A. 2013, A&A, 553, A24
Gies, D. R., & Lambert, D. L. 1992, ApJ, 387, 673
Gray, D. F. 2005, The Observation and Analysis of Stellar Photospheres, 3rd ed. (Cambridge: Cambridge University Press)
Hauck, B., & Mermilliod, M. 1998, A&AS, 129, 431
Hempel, M., & Holweger, H. 2003, A&A, 408, 1065
Kilian, J. 1992, A&A, 262, 171
Korotin, S. A., Andrievsky, S. M., & Luck, R. E. 1999, A&A, 351, 168
Kurucz, R. L. 1993, Kurucz CD-ROM, No. 13 (Harvard-Smithsonian Center for Astrophysics)
Kurucz, R. L., & Bell, B. 1995, Kurucz CD-ROM, No. 23 (Harvard-Smithsonian Center for Astrophysics)
Lyubimkov, L. S., Lambert, D. L. , Poklad, D. B., Rachkovskaya, T. M., & Rostopchin, S. I. 2013, MNRAS, 428, 3497
Lyubimkov, L. S., Rostopchin, S. I., & Lambert, D. L. 2004, MNRAS, 351, 745
Napiwotzki, R., Schönberner, D., & Wenske, V. 1993, A&A, 268, 653
Niemczura, E., Morel, T., Aerts, C. 2009, A&A, 506, 213
Nieva, M.-F. 2013, A&A, 550, A26
Nieva, M.-F., & Przybilla, N. 2012, A&A, 539, A143
Ozaki, S., & Tokimasa, N. 2005, Annu. Rep. Nishi-Harima Astron. Obs., 15, 15 (in Japanese)
Simón-Díaz, S. 2010, A&A, 510, A22
Takeda, Y. 1991, A&A, 242, 455
Takeda, Y. 1992, PASJ, 44, 309
Takeda, Y. 1995, PASJ, 47, 287
Takeda, Y. 2003, A&A, 402, 343
Takeda, Y., Han, I., Kang, D.-I., Lee, B.-C., & Kim, K.-M. 2008, JKAS, 41, 83
Takeda, Y., & Honda, S. 2005, PASJ, 57, 65
Takeda, Y., & Honda, S. 2015, PASJ, 67, 25
Takeda, Y., Kambe, E., Sadakane, K., & Masuda, S. 2010. PASJ, 62, 1239 (Paper I)
Takeda, Y., Kawanomoto, S., & Ohishi, N. 2014, PASJ, 66, 23
Takeda, Y., Kawanomoto, S., & Sadakane, K. 1998, PASJ, 50, 97
Takeda, Y., & Sadakane, K. 1997, PASJ, 49, 367
Takeda, Y., Sato, B., Omiya, M., & Harakawa, H. 2015, PASJ, 67, 24

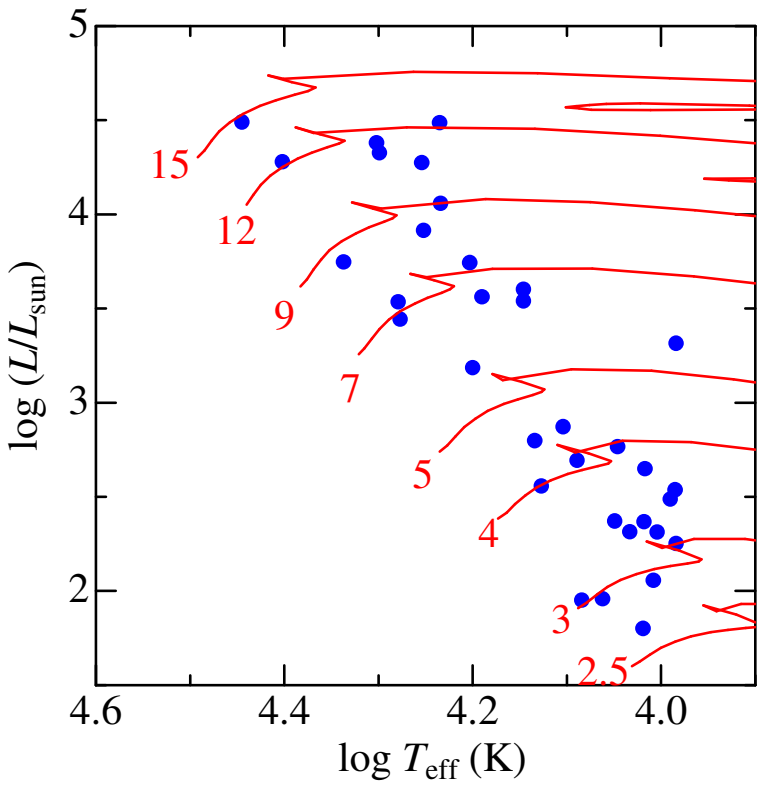

Fig. 1. Plots of the 34 program stars on the theoretical HR diagram ($\log(L/L_{\odot})$ vs. $\log T_{\rm eff}$), where the effective temperature ($T_{\rm eff}$) was determined from $uvby\beta$ photometry as described in section 3 and the bolometric luminosity (L) was evaluated from the apparent visual magnitude, Hipparcos parallax (ESA 1997), Arenou, Grenon, and Gómez's (1992) interstellar extinction map, and Flower's (1996) bolometric correction as in Paper I. Theoretical evolutionary tracks corresponding to the solar metallicity computed by Girardi et al. (2000) for eight different initial masses (2.5, 3, 4, 5, 7, 9, 12, and 15 $M_{\odot}$) are also depicted for comparison.

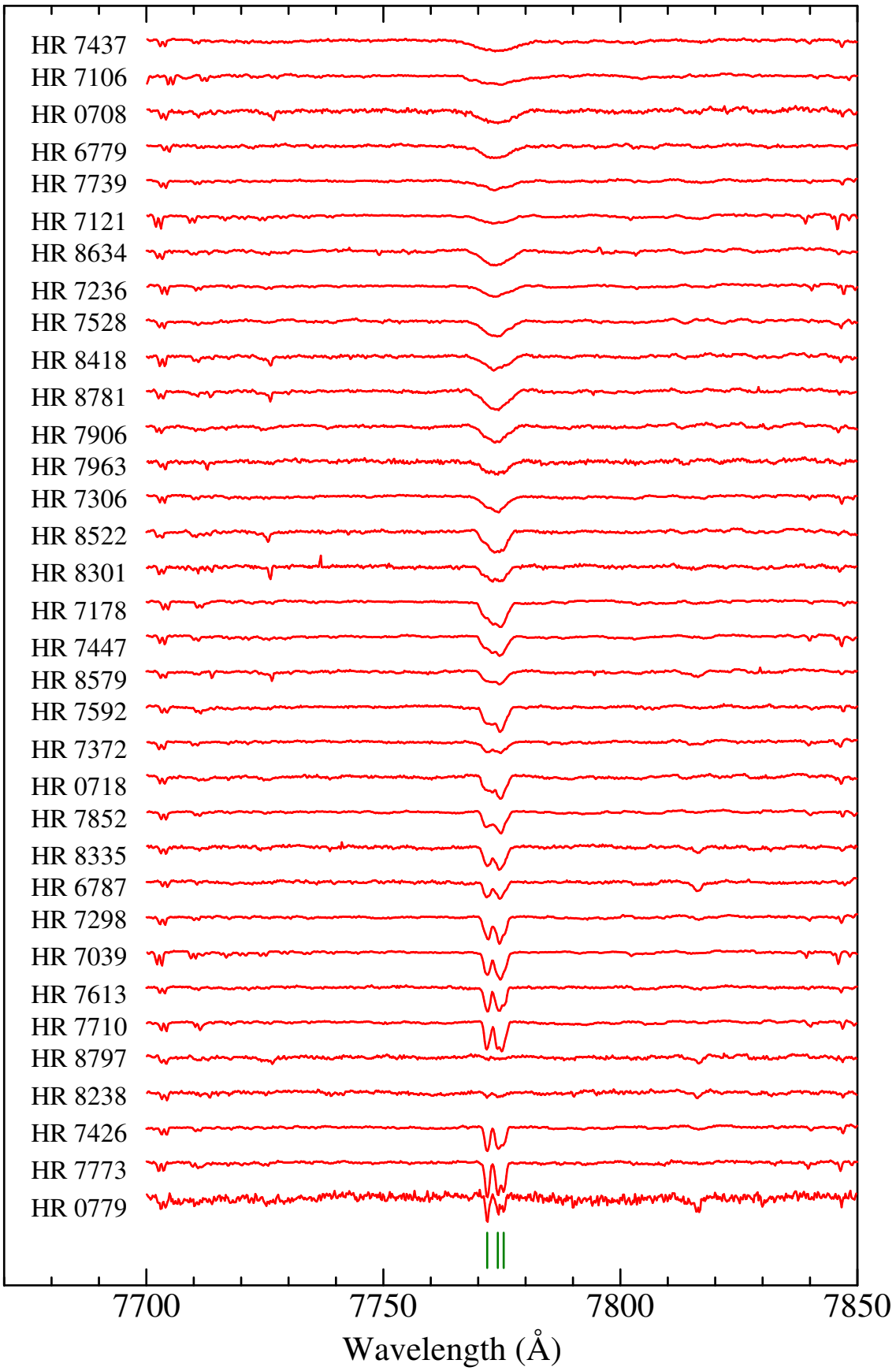

Fig. 2. Observed spectra of 34 B-type stars in the 7700–7850 Å region (normalized with respect to the local continuum), which are arranged in the descending order of $v_{\rm e} \sin i$ (from top to bottom). The wavelength scale is adjusted to the laboratory frame and each spectrum is vertically shifted by 0.2 relative to the adjacent one. The positions of the O I 7771–5 triplet lines are indicated by vertical ticks.

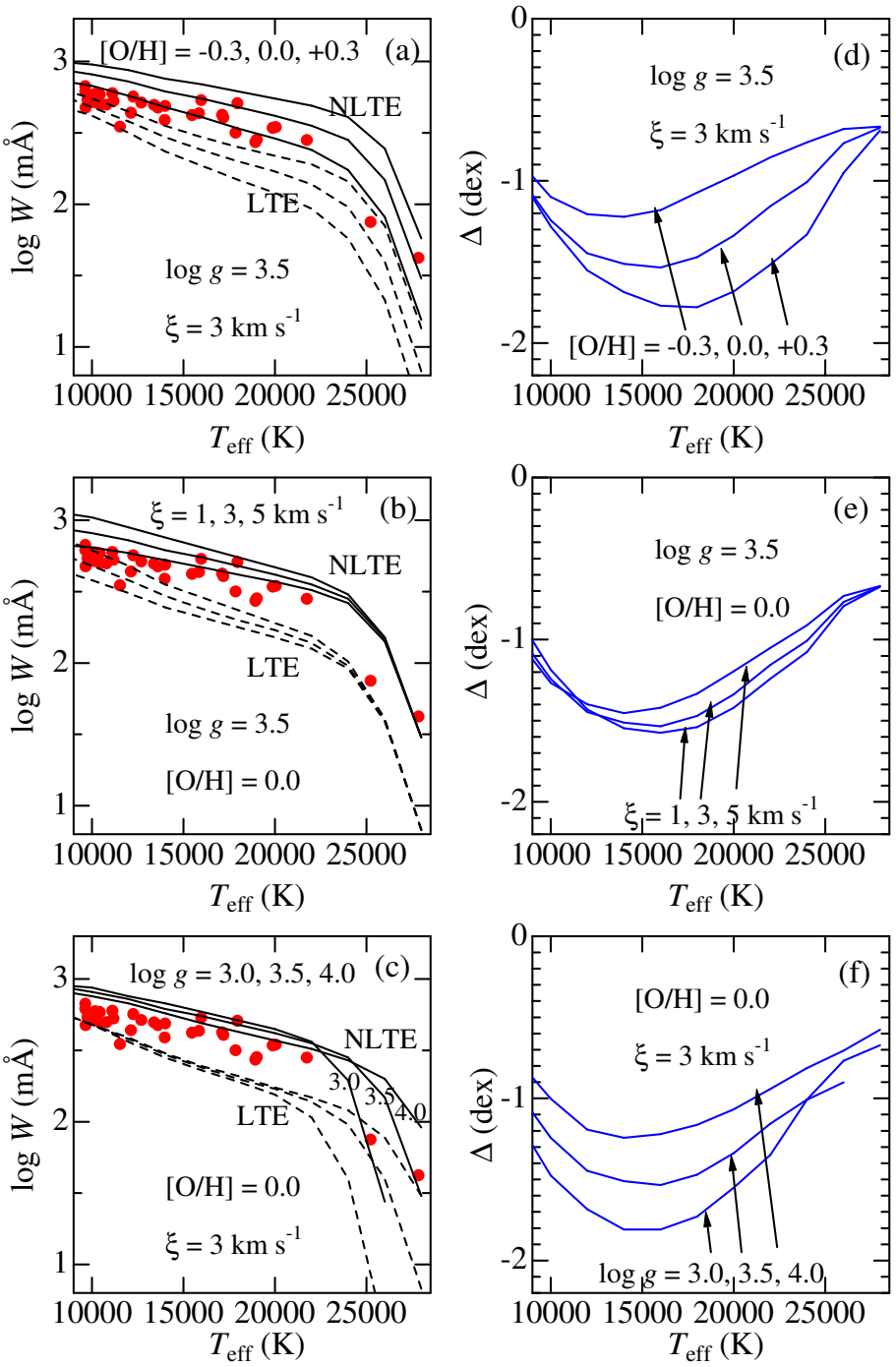

Fig. 3. Non-LTE (solid line) as well as LTE (dashed line) equivalent widths ($\log W$; left panels a–c) and the non-LTE abundance corrections (Δ; right panels d–f) for the total O I 7771–5 triplet lines, which were theoretically computed for representative models and plotted against $T_{\rm eff}$. The upper (a,d), middle (b,e), and bottom (c,f) panels show the effects of changing [O/H], ξ, and $\log g$, respectively. (Note that [O/H] = 0.0 corresponds to $A = 8.93$, as remarked in footnote 5 of section 4.) In the three left panels are also plotted (in filled circles) the W values derived for our 34 targets.

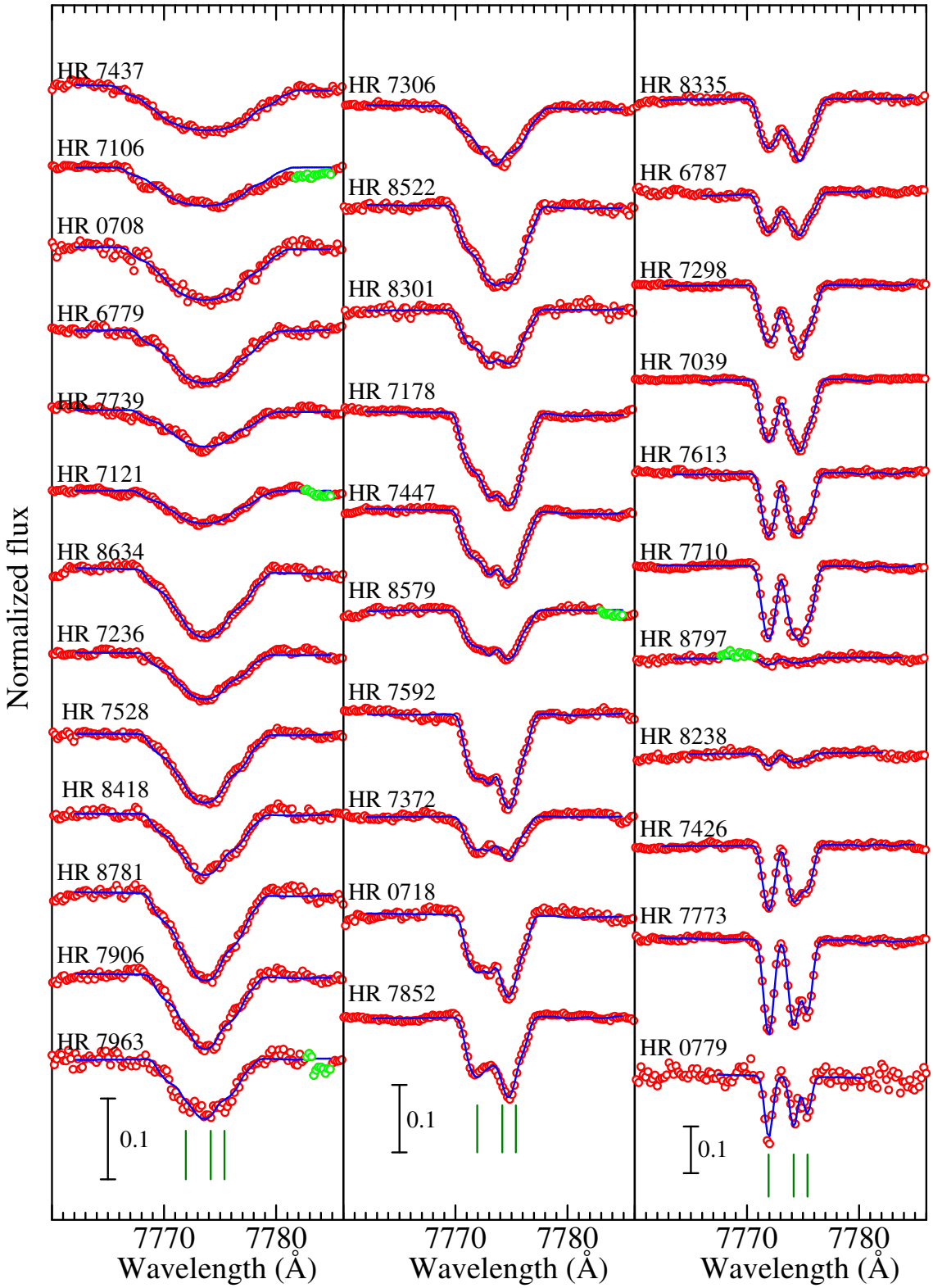

Fig. 4. Synthetic spectrum fitting in the region of O I 7771–5 triplet lines accomplished by varying $v_e \sin i$ and A(O). The best-fit theoretical spectra are shown by blue solid lines. The observed data are plotted by symbols, where those actually used in the fitting are depicted in red, while those rejected are highlighted in green. The spectra are arranged (from top to bottom) in the descending order of $v_e \sin i$ as in table 1, and offset values of 0.1 (left panel), 0.15 (middle panel), and 0.2 (right panel) are applied to each spectrum relative to the adjacent one.

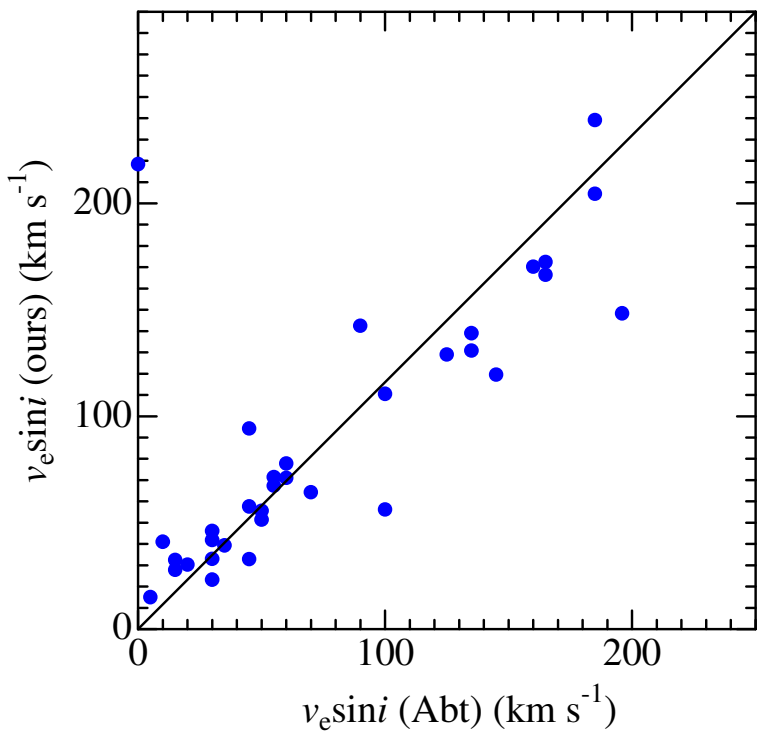

Fig. 5. Comparison of projected rotational velocities ($v_e \sin i$) derived from our analysis with those determined by Abt et al. (2002).

Table 1. Basic data of the program stars and the results of the analysis.

HR#	HD#	Desig.	Sp.type	V	$T_{\rm eff}$	$\log g$	$v_e \sin i$	ξ	W	$A_{\rm N}$	Δ	Obs. date
HR 7437	HD 184606	9 Vul	B8 IIIn	5.00	12703	3.52	239.1	1	515	8.80	−1.40	150731
HR 7106	HD 174638	β Lyr	B8.5 Ib-II	3.52	17124	3.92	218.4	3	422	8.83	−1.14	150612
HR 0708	HD 015130	ρ Cet	A0 V	4.88	9764	3.48	204.5	1	541	8.59	−1.10	150926
HR 6779	HD 166014	o Her	B9.5 III	3.84	9657	3.24	172.4	1	475	8.33	−1.05	150501
HR 7739	HD 192685	···	B3 V	4.79	17855	3.94	170.2	3	317	8.63	−0.88	150815
HR 7121	HD 175191	σ Sgr	B2 V	2.05	19012	4.27	166.4	3	283	8.68	−0.74	150731
HR 8634	HD 214923	ζ Peg	B8 V	3.41	11182	3.65	148.3	1	528	8.70	−1.21	150927
HR 7236	HD 177756	λ Aql	B9 Vn	3.43	11534	4.14	142.5	1	350	8.30	−0.72	150731
HR 7528	HD 186882	δ Cyg	B9.5 IV+.	2.86	10098	3.67	139.0	1	518	8.59	−1.05	150926
HR 8418	HD 209819	ι Aqr	B8 V	4.29	12138	4.26	130.8	1	437	8.65	−0.93	150927
HR 8781	HD 218045	α Peg	B9 III	2.49	9643	3.52	129.0	1	618	8.82	−1.12	150927
HR 7906	HD 196867	α Del	B9 IV	3.77	10794	3.89	119.5	1	497	8.62	−1.03	150926
HR 7963	HD 198183	λ Cyg	B5 V	4.53	13982	3.89	110.5	1	389	8.63	−1.11	150927
HR 7306	HD 180554	1 Vul	B4 IV	4.76	15474	3.78	94.2	3	421	8.68	−1.10	150731
HR 8522	HD 212097	32 Peg	B9 III	4.78	11119	3.44	77.8	1	599	8.86	−1.36	150927
HR 8301	HD 206672	π^1 Cyg	B3 III	4.69	17191	3.55	71.4	3	405	8.73	−1.22	150927
HR 7178	HD 176437	γ Lyr	B9 III	3.25	9638	2.73	71.0	1	670	8.84	−1.43	150612
HR 7447	HD 184930	ι Aql	B5 III	4.36	13400	3.69	67.3	1	497	8.84	−1.37	150731
HR 8579	HD 213420	6 Lac	B2 IV	4.52	19885	3.67	64.3	3	343	8.79	−1.08	150927
HR 7592	HD 188260	13 Vul	B9.5 III	4.57	10425	3.89	57.6	1	585	8.86	−1.07	150815
HR 7372	HD 182568	2 Cyg	B3 IV	4.99	18937	4.28	56.2	3	272	8.65	−0.71	150801
HR 0718	HD 015318	ξ^2 Cet	B9 III	4.30	10438	4.09	55.6	1	498	8.65	−0.91	150926
HR 7852	HD 195810	ϵ Del	B6 III	4.03	13611	3.68	51.4	1	475	8.80	−1.35	150815
HR 8335	HD 207330	π^2 Cyg	B3 III	4.23	17953	3.23	46.1	3	509	8.94	−1.64	150927
HR 6787	HD 166182	102 Her	B2 IV	4.37	20048	3.45	41.8	3	347	8.77	−1.15	150501
HR 7298	HD 180163	η Lyr	B2.5 IV	4.43	15974	3.19	41.0	3	535	8.85	−1.61	150801
HR 7039	HD 173300	ϕ Sgr	B8 III	3.17	12263	3.66	39.3	1	567	8.92	−1.37	150815
HR 7613	HD 188892	22 Cyg	B5 IV	4.95	14008	3.38	33.0	1	487	8.80	−1.53	150815
HR 7710	HD 191692	θ Aql	B9.5 III	3.24	10410	3.71	32.9	1	585	8.82	−1.14	150815
HR 8797	HD 218376	1 Cas	B0.5 III	4.84	27853	3.64	32.5	3	42	8.86	−0.63	150927
HR 8238	HD 205021	β Cep	B0.5 IIIs	3.23	25231	3.63	30.3	3	75	8.36	−0.60	150927
HR 7426	HD 184171	8 Cyg	B3 IV	4.74	15858	3.54	27.8	3	434	8.69	−1.23	150801
HR 7773	HD 193432	ν Cap	B9 IV	4.77	10180	3.91	23.2	1	595	8.88	−1.03	150801
HR 0779	HD 016582	δ Cet	B2 IV	4.08	21747	3.63	15.0	3	281	8.74	−0.93	150926

Note.
In columns 1 through 8 are given the HR number, HD number, star designation, spectral type, apparent visual magnitude (in mag), effective temperature (in K), logarithmic surface gravity (in cm s^{-2}), and projected rotational velocity (in km s^{-1}; derived from our fitting analysis). Columns 9 through 12 show the results of abundance analysis: assigned microturbulence (cf. section 3), total equivalent width of the O I 7771–5 lines (in mÅ), non-LTE O abundance (in dex; expressed in the usual normalization of H=12.00), and non-LTE correction (in dex). Column 13 gives the observation date (for example, 150907 means 2015 September 7). The objects are arranged in the descending order of $v_e \sin i$.

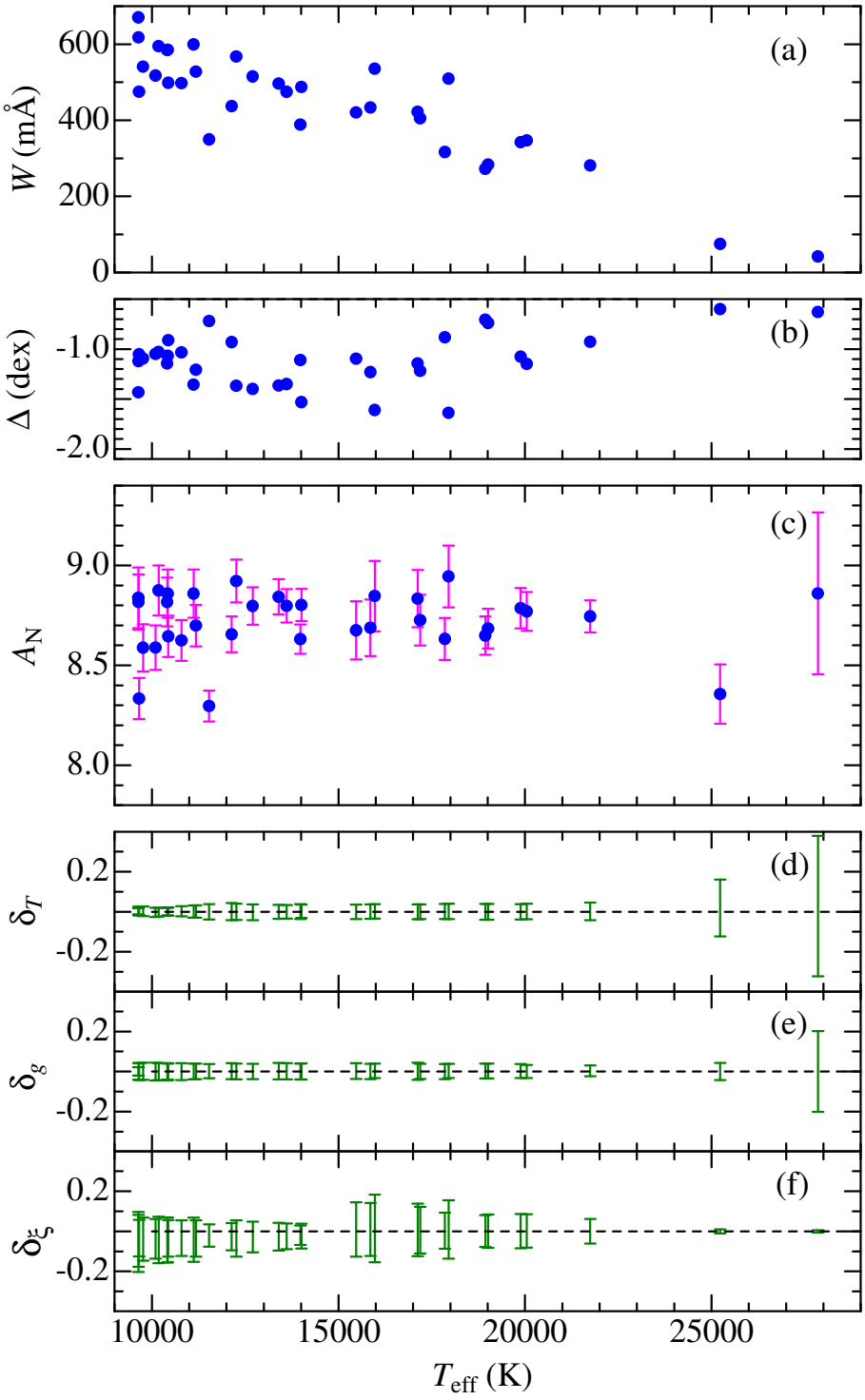

Fig. 6. Oxygen abundances along with the abundance-related quantities specific to the O I 7771–5 feature, plotted against $T_{\rm eff}$. (a) W (total equivalent width of the triplet), (b) Δ (non-LTE correction), (c) $A_{\rm N}$ (non-LTE oxygen abundance, where the attached error bar is $\delta_{Tg\xi}$), (d) δ_{T+} and δ_{T-} (abundance variations in response to $T_{\rm eff}$ changes), (e) δ_{g+} and δ_{g-} (abundance variations in response to $\log g$ changes), and (f) $\delta_{\xi+}$ and $\delta_{\xi-}$ (abundance variations in response to ξ changes). See subsection 5.3 for more detailed explanations regarding the δ values. The signs of δ's concerning the variations of $T_{\rm eff}$ and ξ are are $\delta_{T+} > 0$, $\delta_{T-} < 0$, $\delta_{\xi+} < 0$, and $\delta_{\xi-} > 0$. Regarding the sensitivity to $\log g$, $\delta_{g+} > 0$ and $\delta_{g-} < 0$ for most stars, but the sign is reversed for the two stars at $T_{\rm eff} > 25000$ K.

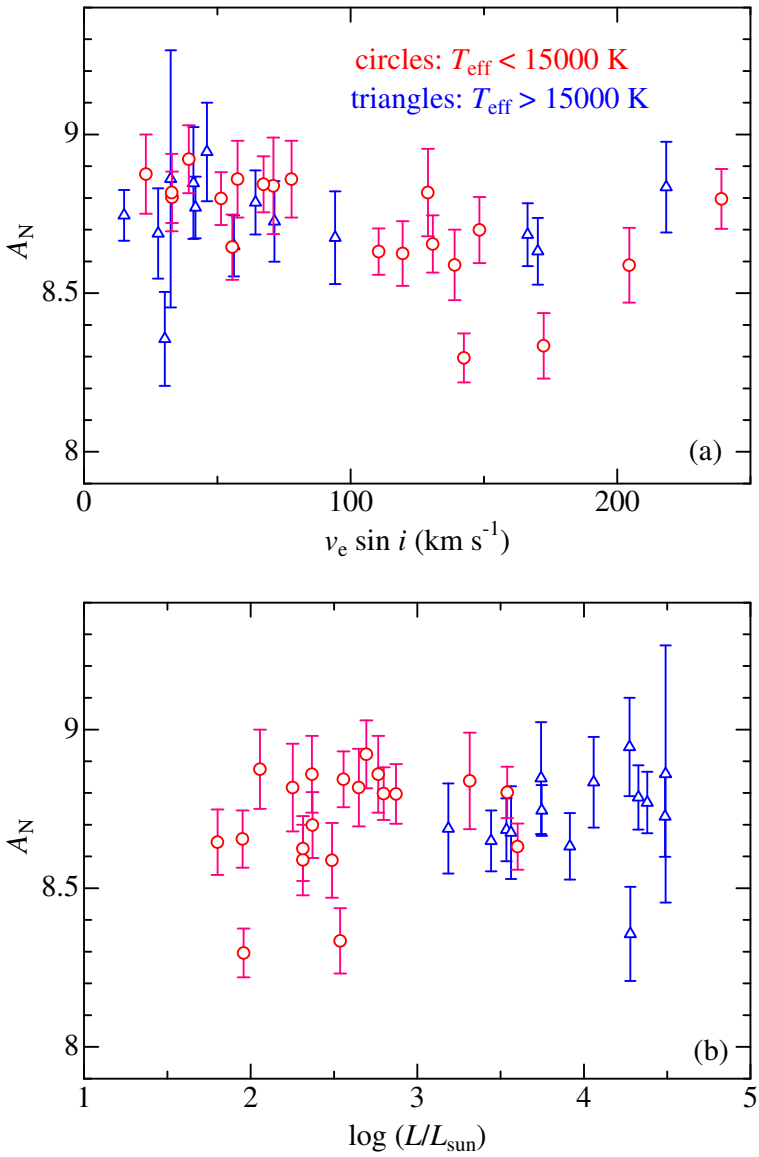

Fig. 7. Oxygen abundances of 34 B-type stars plotted against (a) $v_{\rm e} \sin i$ and (b) $\log L$ (cf. figure 1). where stars of $T_{\rm eff} < 15000$ K and $T_{\rm eff} > 15000$ K, are expressed in open circles and open triangles, respectively. The data and the attached error bars are the same as in figure 6c.

Table 2. Adopted atomic data of O I 7771–5 lines.

Species	$\lambda_{\rm air}$ (Å)	$\chi_{\rm low}$ (eV)	$\log gf$ (dex)	Gammar (dex)	Gammas (dex)	Gammaw (dex)
O I	7771.944	9.146	+0.324	7.52	−5.55	(−7.65)
O I	7774.166	9.146	+0.174	7.52	−5.55	(−7.65)
O I	7775.388	9.146	−0.046	7.52	−5.55	(−7.65)

Note.
The first four columns are self-explanatory. Presented in columns 5–7 are the damping parameters: Gammar is the radiation damping width (s^{-1}) [$\log\gamma_{\rm rad}$], Gammas is the Stark damping width (s^{-1}) per electron density (cm^{-3}) at 10^4 K [$\log(\gamma_{\rm e}/N_{\rm e})$], and Gammaw is the van der Waals damping width (s^{-1}) per hydrogen density (cm^{-3}) at 10^4 K [$\log(\gamma_{\rm w}/N_{\rm H})$].
These data were taken from the compilation of Kurucz and Bell (1995) as long as available, while the parenthesized damping parameters are the default values computed by the WIDTH9 program.